Heat and Mass Transfer 36 (2000) 257 – 264 © Springer-Verlag 2000

Numerical simulation of heat transfer induced by a body moving in the same direction as flowing fluids

W.-S. Fu, S.-J. Yang

Abstract Variations of flow field and heat transfer induced by a body moving in the same direction as flowing fluids in a channel were studied numerically. This situation is cataloged to a kind of moving boundary problem and an arbitrary Lagrangian–Eulerian description method with a Galerkin finite element formulation is adopted to analyze this problem. Several different moving velocities of the body and Reynolds numbers are taken into consideration. The results show that the fluids simultaneously complement the vacant space induced by the movement of the body and new recirculation zones are formed near the body. These phenomena are remarkably different from those of the moving body regarded as a stationary body in the flowing fluids by a relative velocity viewpoint. Heat transfer rates of the body are enhanced significantly as the body moves rapidly, but the slight enhancement is indicated as the body moves slower than the flowing fluids. In the computing range, the mean global Nusselt numbers $\overline{\mathrm{Nu}}$ can be approximately expressed as the form of $\overline{\mathrm{Nu}} = 0.62\,\mathrm{Re}^{*1/2} - 2.95$.

List of symbols

h	dimensional height of the channel, m
H	dimensionless height of the channel
d	dimensional distance from the outlet of the channel to the bottom surface of the body, m
D	dimensionless distance from the outlet of the channel to the bottom surface of the body
L	dimensionless length of the body
N_i	shape function
n_e	number of elements
Nu	average global Nusselt number
$\overline{\mathrm{Nu}}$	mean global Nusselt number
Nu_X	local Nusselt number on the top or bottom surface of the body
$\overline{\mathrm{Nu}_X}$	average local Nusselt number on the top or bottom surface of the body
Nu_Y	local Nusselt number on the lateral surface of the body
$\overline{\mathrm{Nu}_Y}$	average local Nusselt number on the lateral surface of the body
p	dimensional pressure, $\mathrm{N/m^2}$
p_∞	reference pressure, $\mathrm{N/m^2}$
P	dimensionless pressure
Pr	Prandtl number
Re	Reynolds number
Re^*	special Reynolds number
t	dimensional time, s
T	dimensional temperature, K
T_b	dimensional temperature of the body, K
T_0	dimensional temperature of the inlet fluids, K
u, v	dimensional velocities in x and y directions, m/s
U, V	dimensionless velocities in X and Y directions
v_0	dimensional velocity of the inlet fluids, m/s
v_b	dimensional moving velocity of the body in y-direction, m/s
V_b	dimensionless moving velocity of the body in Y-direction
$\hat{v}$	dimensional mesh velocity in y-direction, m/s
$\hat{V}$	dimensionless mesh velocity in Y-direction
w	dimensional width of the channel, m
W	dimensionless width of the channel
x, y	dimensional Cartesian coordinates, m
X, Y	dimensionless Cartesian coordinates

Greek symbols

α	thermal diffusivity, $\mathrm{m^2/s}$
ϕ	computational variables
ι	dimensional length of the body, m
λ	penalty parameter
ν	kinematic viscosity, $\mathrm{m^2/s}$
θ	dimensionless temperature
τ	dimensionless time

Superscripts

(e)	element
m	iteration number
T	transpose matrix

Others

[ ]	matrix
{ }	column vector
⟨ ⟩	row vector
| |	absolute value

Received on 13 July 1999

W.-S. Fu, S.-J. Yang
Department of Mechanical Engineering
National Chiao Tung University, 1001 Ta Hsueh Road
Hsinchu, 30056, Taiwan

Correspondence to: W.-S. Fu

The support of this work by National Science Council, Taiwan, R.O.C. under contract NSC87-2212-E-009-035 is gratefully acknowledged.

1 Introduction

The variations of the flow and thermal fields caused by the interaction between a moving body and flowing fluids are important and interesting in many practical engineering applications. Previous studies related to this subject were conventionally regarded the moving body as a stationary body in flowing fluids by a concept of the relative velocity. However, for holding the continuity equation, the fluids near the body simultaneously complement the vacant space induced by the movement of the body. Strictly speaking, the moving body regarded as the stationary body in the flowing fluids is different from that of the body moving in the flowing fluids. Hence, the later situation mentioned above is hardly analyzed by either the Lagrangian or Eulerian description method solely, and can be classified into a kind of moving boundary problems.

In the past, Hirt et al. [1] adopted an arbitrary Lagrangian–Eulerian (ALE) method, which combined the characteristics of the Lagrangian and Eulerian formulations, to solve fluid dynamics problems with moving boundaries. The basic methodology, stability, accuracy, and rezoning of the ALE method were described in detail. Hughes et al. [2], Ramaswamy [3] and Soulaimani and Saad [4] utilized the ALE method to solve the incompressible flow with free surface. A general kinematic theory for the ALE method was discussed clearly.

Furthermore, the ALE method was adopted to simulate the fluid-structure interaction [5–8], material forming process [9, 10] and solid mechanics problems [11, 12]. The solutions obtained by ALE method were consistent well with the previous or experimental results.

Based upon the literature mentioned above, most of the studies were focused on the variations of the flow fields. However, in many engineering applications, such as heat exchanger, moving machine and fluid machinery, the variations of both the flow and thermal fields of the moving boundary problems are important, but little attention has been devoted to this subject.

Hence, in this study, the ALE method is adopted to investigate the variations of the flow and thermal fields induced by a body moving in the same direction as flowing fluids numerically. For avoiding the distortion and deformation of computational meshes due to a long movement of the body, an interpolation method is used to reconstruct the distortion and deformation computational meshes if necessary. A Galerkin finite element method and an implicit scheme dealing with the time terms are adopted to solve the governing equations. The results show that the moving body dominates the variations of the flow fields, and heat transfer rates are increased apparently as the velocity of the moving body is fast.

2 Physical model

A two-dimensional vertical channel with height h and width w, respectively, as sketched in Fig. 1 is used. A square body with length ι is set within the channel. FH and EG are the top and bottom surfaces of the body, respectively, FE and HG are the lateral surfaces of the body. The distance from the outlet of the channel to the bottom

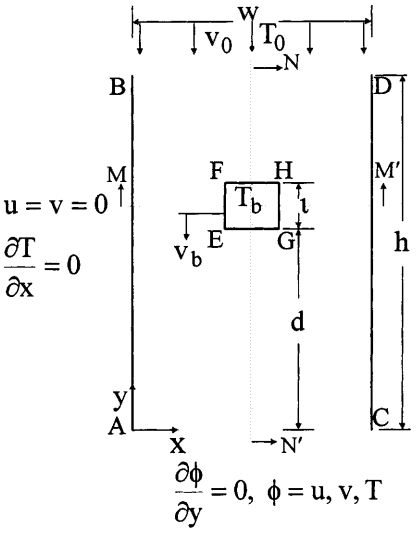

Fig. 1. The physical model

surface of the body is d. The inlet velocity and temperature of the fluids are constant and equal to v_0 and T_0, respectively. The body is maintained at temperature T_b, which is higher than T_0. Initially ($t = 0$), the body is stationary and fluids flow steadily. As time $t > 0$, the body starts to move downward with a constant velocity v_b, which is in the same direction as the inlet fluids. The behavior of the body and fluids are then affected mutually, and the variations of the flow and thermal fields become time-dependent and can be classified into a kind of moving boundary problems. As a result, the ALE method is properly utilized to analyze this problem.

In order to facilitate the analysis, the following assumptions and the dimensionless variables are made.

1. The fluid is air and the flow field is two-dimensional, incompressible and laminar.
2. The fluid properties are constant and the effect of the gravity is neglected.
3. The no-slip conditions is held on the interface between the fluids and body.

$$X = \frac{x}{\iota}, \quad Y = \frac{y}{\iota}, \quad U = \frac{u}{v_0}, \quad V = \frac{v}{v_0},$$
$$\hat{V} = \frac{\hat{v}}{v_0}, \quad V_b = \frac{v_b}{v_0}, \quad P = \frac{p - p_\infty}{\rho v_0^2}, \quad \tau = \frac{t v_0}{\iota}, \qquad (1)$$
$$\theta = \frac{T - T_0}{T_b - T_0}, \quad \mathrm{Re} = \frac{v_0 \iota}{\nu}, \quad \mathrm{Pr} = \frac{\nu}{\alpha}.$$

Based upon the above assumptions and dimensionless variables, the dimensionless ALE governing equations [2–4] are expressed as the following equations:
Continuity equation

$$\frac{\partial U}{\partial X} + \frac{\partial V}{\partial Y} = 0 \qquad (2)$$

Momentum equations

$$\frac{\partial U}{\partial \tau} + U\frac{\partial U}{\partial X} + (V - \hat{V})\frac{\partial U}{\partial Y} = -\frac{\partial P}{\partial X} + \frac{1}{\mathrm{Re}}\left(\frac{\partial^2 U}{\partial X^2} + \frac{\partial^2 U}{\partial Y^2}\right) \qquad (3)$$

$$\frac{\partial V}{\partial \tau} + U\frac{\partial V}{\partial X} + (V - \hat{V})\frac{\partial V}{\partial Y} = -\frac{\partial P}{\partial Y} + \frac{1}{\mathrm{Re}}\left(\frac{\partial^2 V}{\partial X^2} + \frac{\partial^2 V}{\partial Y^2}\right) \tag{4}$$

Energy equation

$$\frac{\partial \theta}{\partial \tau} + U\frac{\partial \theta}{\partial X} + (V - \hat{V})\frac{\partial \theta}{\partial Y} = \frac{1}{\mathrm{Pr}\,\mathrm{Re}}\left(\frac{\partial^2 \theta}{\partial X^2} + \frac{\partial^2 \theta}{\partial Y^2}\right) \tag{5}$$

As $\tau > 0$, the boundary conditions are as follows:
on the surfaces AB and CD

$$U = V = 0, \quad \partial\theta/\partial X = 0 \tag{6}$$

on the surface BD

$$U = 0, \quad V = 1, \quad \theta = 0 \tag{7}$$

on the surface AC

$$\partial U/\partial Y = \partial V/\partial Y = \partial\theta/\partial Y = 0 \tag{8}$$

on the interfaces EF, FH, EG and GH between the fluids and body

$$U = 0, \quad V = V_\mathrm{b}, \quad \theta = 1 \tag{9}$$

3 Numerical method

A Galerkin finite element method and an implicit scheme dealing with the time terms are adopted to solve the governing equations (2)–(5). Newton–Raphson iteration algorithm and a penalty function [13] are utilized to handle the nonlinear and pressure terms in the momentum equations, respectively. The velocity and temperature terms are expressed as quadrilateral and nine-node quadratic isoparametric elements. The discretization process of the governing equations is similar to the one used in Fu et al. [14]. Then, the momentum equations (3) and (4) can be expressed as follows:

$$\sum_1^{n_\mathrm{e}}\left([A]^{(\mathrm{e})} + [K]^{(\mathrm{e})} + \lambda[L]^{(\mathrm{e})}\right)\{q\}^{(\mathrm{e})}_{\tau+\Delta\tau} = \sum_1^{n_\mathrm{e}}\{f\}^{(\mathrm{e})} \tag{10}$$

in which

$$\left(\{q\}^{(\mathrm{e})}_{\tau+\Delta\tau}\right)^{\mathrm{T}} = \langle U_1, U_2, \ldots, U_9,\ V_1, V_2, \ldots, V_9\rangle^{m+1}_{\tau+\Delta\tau} \tag{11}$$

where, $[A]^{(\mathrm{e})}$ including the (m)th iteration values of U and V at time $\tau + \Delta\tau$. $[K]^{(\mathrm{e})}$ including the shape function, $\hat{V}$ and time differential terms. $[L]^{(\mathrm{e})}$ including the penalty function terms. $\{f\}^{(\mathrm{e})}$ including the known values of U and V at time τ and (m)th iteration values of U and V at time $\tau + \Delta\tau$.

The energy equation (5) can be expressed as follows:

$$\sum_1^{n_\mathrm{e}}\left([M]^{(\mathrm{e})} + [Z]^{(\mathrm{e})}\right)\{c\}^{(\mathrm{e})}_{\tau+\Delta\tau} = \sum_1^{n_\mathrm{e}}\{r\}^{(\mathrm{e})} \tag{12}$$

where

$$\left(\{c\}^{(\mathrm{e})}_{\tau+\Delta\tau}\right)^{T} = \langle\theta_1, \theta_2, \ldots, \theta_9\rangle_{\tau+\Delta\tau} \tag{13}$$

in which, $[M]^{(\mathrm{e})}$ including the values of U and V at time $\tau + \Delta\tau$. $[Z]^{(\mathrm{e})}$ including the shape function, $\hat{V}$ and time differential terms. $\{r\}^{(\mathrm{e})}$ including the known values of θ at time τ.

In Eqs. (10) and (12), the terms which include the penalty function are integrated by 2×2 Gaussian quadrature, and the other terms are integrated by 3×3 Gaussian quadrature. The value of penalty parameter, λ, used in this study is 10^6 and the frontal method is utilized to solve Eqs. (10) and (12).

For holding the boundary conditions to be satisfied at the inlet and outlet of the computational domain as shown in Fig. 1, the displacement of the body is then limited, and do not disturb the boundary conditions mentioned previously.

Concerning the mesh velocity $\hat{V}$, it is linear distribution and inverse proportion to the distance between the node of the computational meshes and the body in this study. The mesh velocity near the body is faster than that near the boundary of the computational domain. In addition, the boundary layer thickness on the body surface is extremely thin and can be approximately estimated by $\mathrm{Re}^{-1/2}$ [15]. To avoid the computational nodes in the vicinity of the body to slip away the boundary layer, the meshes velocities adjacent to the body are expediently assigned equal to the velocity of the body.

A brief outline of the solution procedure are described as follows:

1. Determine the optimal mesh distribution and number of the elements and nodes.
2. Solve the values of the U, V and θ at the steady state and regard them as the initial values.
3. Determine the time increment $\Delta\tau$ and the mesh velocities of the computational meshes.
4. Update the coordinates of the nodes and examine the determinant of the Jacobian transformation matrix to ensure the one-to-one mapping to be satisfied during the Gaussian quadrature numerical integration, execute the mesh reconstruction if necessary.
5. Solve Eq. (10), until the following criteria for convergence are satisfied:

$$\left|\frac{\phi^{m+1} - \phi^m}{\phi^{m+1}}\right|_{\tau+\Delta\tau} < 10^{-3}, \quad \text{where } \phi = U, V \tag{14}$$

6. Substitute the U and V into Eq. (12) to obtain θ.
7. Continue the next time step calculation until the assigned time reaches.

4 Results and discussion

The working fluid is air with Pr = 0.71. For matching the boundary conditions at the inlet and outlet of the channel mentioned previously, at the time $\tau = 0.0$ the dimensionless lengths of $H(=h/\imath)$ and $D(=d/\imath)$ are determined by the numerical tests and equal to 30 and 20, respectively. The dimensionless width $W(=w/\imath)$ of the channel is 10, and the dimensionless length $L(=\imath/\imath)$ of the body is 1.

The local Nusselt number Nu_X and the average local Nusselt number $\overline{\mathrm{Nu}_X}$ on the top surface (FH) and the

bottom surface (EG) of the body at the time τ are defined as follows, respectively.

$$\mathrm{Nu}_X = -\frac{\partial\theta}{\partial Y} \tag{15}$$

$$\overline{\mathrm{Nu}_X} = \frac{1}{L}\int_0^L \mathrm{Nu}_X \, \mathrm{d}X \tag{16}$$

The local Nusselt number Nu_Y and the average local Nusselt number $\overline{\mathrm{Nu}_Y}$ on the lateral surface (EF or GH) of the body at the time τ are defined as follows, respectively.

$$\mathrm{Nu}_Y = -\frac{\partial\theta}{\partial X} \tag{17}$$

$$\overline{\mathrm{Nu}_Y} = \frac{1}{L}\int_0^L \mathrm{Nu}_Y \, \mathrm{d}Y \tag{18}$$

The average global Nusselt number Nu on the surfaces of the body at the time τ is defined as

$$\mathrm{Nu} = \frac{1}{4L}\left(\int_{FH} \mathrm{Nu}_X \, \mathrm{d}X + \int_{EG} \mathrm{Nu}_X \, \mathrm{d}X + \int_{EF+GH} \mathrm{Nu}_Y \, \mathrm{d}Y\right) \tag{19}$$

The mean global Nusselt number $\overline{\mathrm{Nu}}$ in the duration of the transient developments on the surface of the body is defined as

$$\overline{\mathrm{Nu}} = \frac{1}{\tau}\int_0^\tau \mathrm{Nu} \, \mathrm{d}\tau \tag{20}$$

In order to obtain the optimal computational meshes, three different nonuniform element distributions of 1872, 2672 and 3904 (corresponding to 7720, 10952 and 15944 nodes) are used for the grid tests at steady state and Re = 500 situation. The results of U, V and θ distributed along the lines MM′ and NN′ as shown in Fig. 1 are indicated in Fig. 2. According to the results of the grid tests, the meshes with 3904 elements (15944 nodes) are adopted for the computation. Besides, the time step $\Delta\tau = 5 \times 10^{-3}$ is adopted by the time step tests and the total computational time τ changing from 0 to 1 is considered in this study.

Due to the limitation of contents, the flow and heat transfer mechanisms are mainly focused on the velocities of the body $V_b = -0.5$ and -2.0 under Re = 500 situation. For illustrating the flow and thermal fields more clearly, the phenomena in the vicinity of the body are presented only.

The transient developments of the velocity vectors around the body for $V_b = -0.5$ case are shown in Fig. 3. At the steady state ($\tau = 0.0$), recirculation zones neighboring the bottom surface of the body and reverse flow zones near the lateral surface of the body are observed apparently. At the beginning of the transient state, the body moves downward and presses the fluids of which the flowing direction is upward near the bottom surface of the body, and the flowing direction of these fluids is

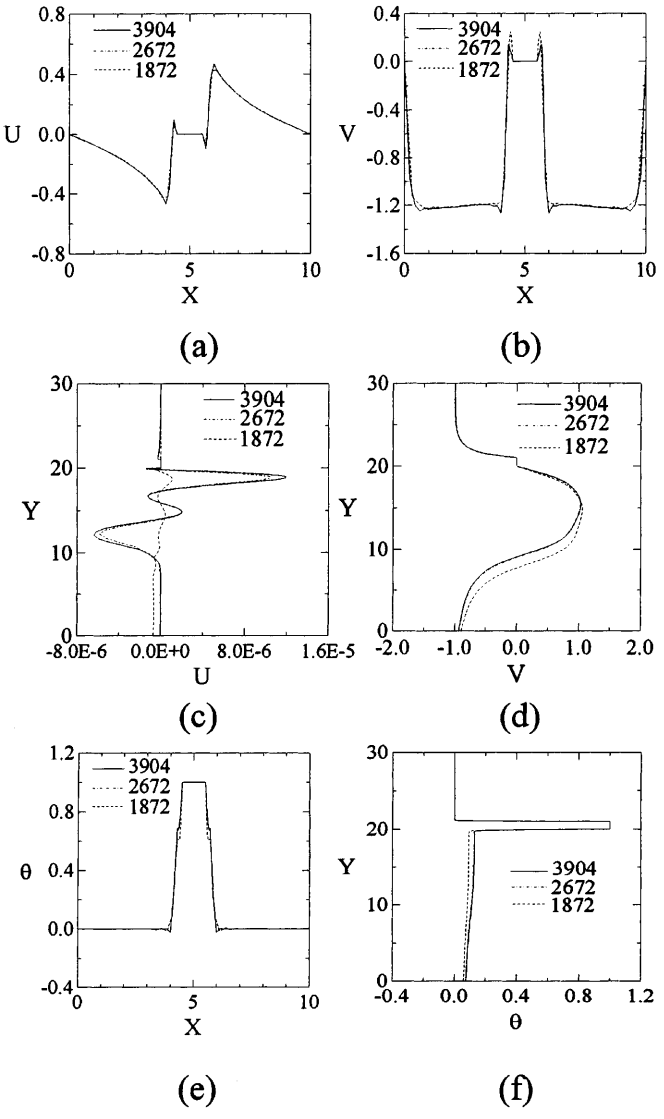

Fig. 2. Comparison of the steady U, V and θ distributions along the lines MM′ and NN′ and Re = 500 for various grids

forced to change drastically and turned to the two sides of the bottom surface of the body. From a relative velocity viewpoint, the behavior is similar to the fluids impinging on the bottom surface of the body, which is advantageous to heat transfer.

As for the fluids near the top surface of the body, because the approaching velocity of the fluids is flowing downward which is in the same direction as the moving body, the impinging effect caused by the fluids impinging on the top surface at the steady state is more apparent than that during the transient development, which is disadvantageous to heat transfer.

Concerning the behavior of the fluids near the lateral surface of the body, as the body begins to move downward, the fluids near the corner of the bottom surface of the body are pressed by the body which causes the reverse flow near the lateral surface of the body to be more apparent at first. Afterward, recirculation zones appear around the lower corners of the lateral surface, and reattachment regions exist on the lateral surface, which is profitable for the heat

transfer mechanism. As the time increases, the movement of the body affects the fluids near the lateral surface and the flow direction of the fluids is forced to change gradually. Finally, most of the fluids close to the lateral surface are flowing with the lateral surface.

Shown in Fig. 4, there are transient developments of the isothermal lines around the body for $V_b = -0.5$ case. Since the fluids impinge on the bottom surface of the body during the transient state mentioned above, the distributions of the isothermal lines are dense near the bottom surface of the body. As for the distribution of the isothermal lines near the top surface of the body, these distributions become sparse gradually, the reason is that the impinging effect of the fluids on the top surface becomes weak, which is disadvantageous to heat transfer. As for the distributions of the isothermal lines near the lateral surface of the body, the flow fields near the lateral surface is affected by the movement of the body remarkably, which results in the density of the isothermal lines distributed near the lateral surface varying drastically. Moreover, the isothermal lines near the reattachment region are denser in the neighborhood of the lateral surface.

The results of the transient developments of the local Nusselt numbers Nu_X and Nu_Y on the surfaces of the body for $V_b = -0.5$ case are indicated in Figs. 5 and 6, respectively. The solid and dashed lines in Fig. 5 indicate the results of the top and bottom surfaces of the body, respectively. As the body starts to move downward, the fluids near the bottom surface of the body pressed by the body mentioned earlier are similar to an impinging flow that enhances the heat transfer rate on the bottom surface. On the top surface of the body, most of the fluids no longer strongly impinge on the top surface during the transient developments. Consequently, the distributions of the local Nusselt numbers on the top surface during the transient developments are smaller than those at the steady state. The magnitude of decrement of the local Nusselt numbers at both the corners of the top surface are remarkable because of the edge effect of the corners being weak in the duration of the transient developments.

In Fig. 6, the results of the local Nusselt number Nu_Y on the lateral surface of the body are shown. At the steady state (Fig. 6a), the situation is similar to the fluids flowing through a plate with finite length, and the larger local

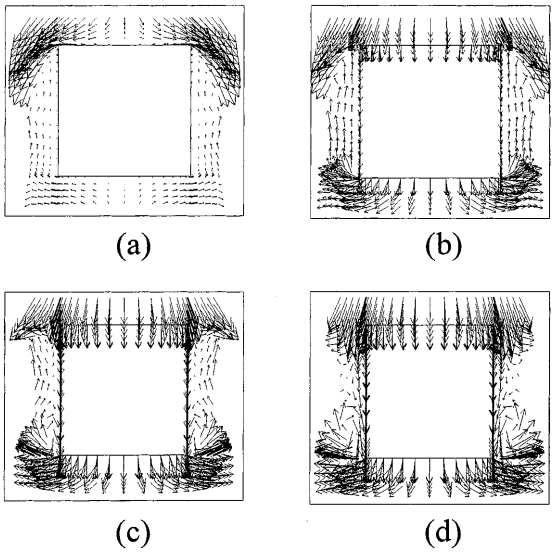

Fig. 3a–d. The transient developments of the velocity vectors around the body for Re = 500 and $V_b = -0.5$ case **a** $\tau = 0.0$, **b** $\tau = 0.05$, **c** $\tau = 0.5$, **d** $\tau = 1.0$

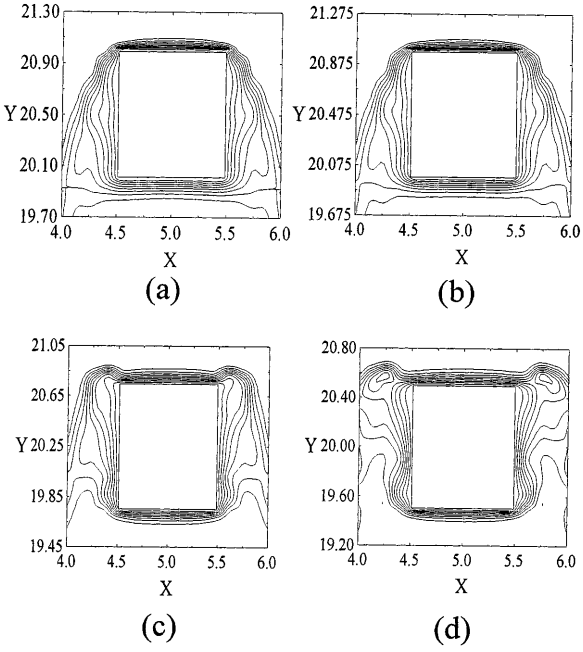

Fig. 4a–d. The transient developments of the isothermal lines around the body for Re = 500 and $V_b = -0.5$ case **a** $\tau = 0.0$, **b** $\tau = 0.05$, **c** $\tau = 0.5$, **d** $\tau = 1.0$

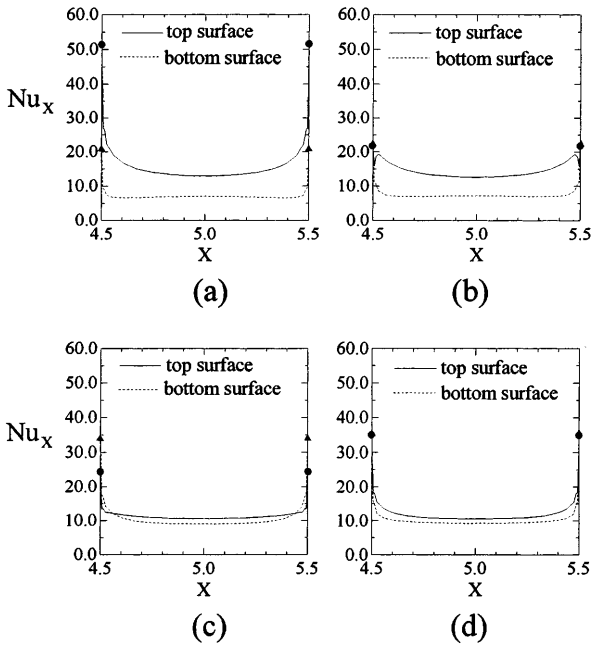

Fig. 5a–d. The transient developments of the local Nusselt numbers Nu_X on the top and bottom surfaces for Re = 500 and $V_b = -0.5$ case **a** $\tau = 0.0$, **b** $\tau = 0.05$, **c** $\tau = 0.5$, **d** $\tau = 1.0$

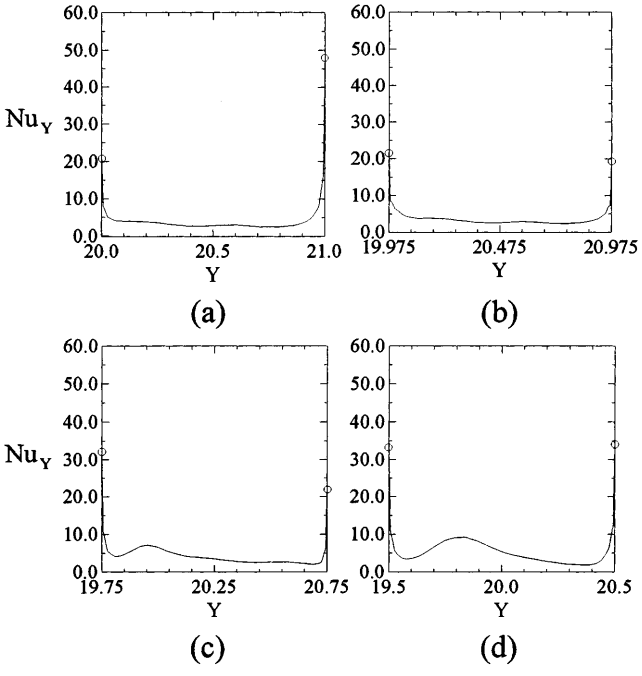

Fig. 6a–d. The transient developments of the local Nusselt numbers Nu_Y on the lateral surface of the body for Re = 500 and $V_b = -0.5$ case **a** $\tau = 0.0$, **b** $\tau = 0.05$, **c** $\tau = 0.5$, **d** $\tau = 1.0$

Nusselt numbers are distributed on the upper and lower edges of the lateral surface of the body. As the body starts to move downward, the relative velocity of the fluids flowing over the upper edge of the lateral surface is reduced, then the local Nusselt numbers on the upper edge of the lateral surface are decreased remarkably at first. Oppositely, the local Nusselt numbers on the lower edge of the lateral surface of the body are increased significantly due to the fluids with higher velocity flowing over the corner of the bottom surface of the body mentioned earlier. A rising distribution of the local Nusselt numbers on the center regions indicates the reattachment regions and varies with time.

The transient developments of the average local Nusselt numbers $\overline{Nu_X}$ and $\overline{Nu_Y}$ on the surfaces of the body for $V_b = -0.5$ case are shown in Fig. 7. Based upon the reasons mentioned above, the average local Nusselt numbers on the bottom surface of the body during the transient developments are larger than those at the steady state. Oppositely, the average local Nusselt numbers on the top surface of the body under the transient state are smaller than those at the steady state. As for the lateral surface of the body, the average local Nusselt numbers decrease at first and increase a little with the increment of time. According to the variations of heat transfer mentioned above, the mean increment of the average global Nusselt numbers Nu is not significant.

Shown in Fig. 8, there are the transient developments of the velocity vectors around the body for $V_b = -2.0$ case. The variations of the flow fields near the body are more drastic since the moving velocity of the body in this case is greater than that of the above case ($V_b = -0.5$). The flow fields near the bottom and lateral surfaces of the body in this case are similar to those of the $V_b = -0.5$ case. As

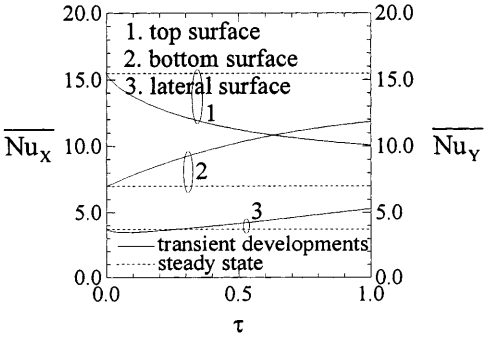

Fig. 7. The transient developments of the average local Nusselt numbers on the surfaces of the body for Re = 500 and $V_b = -0.5$ case

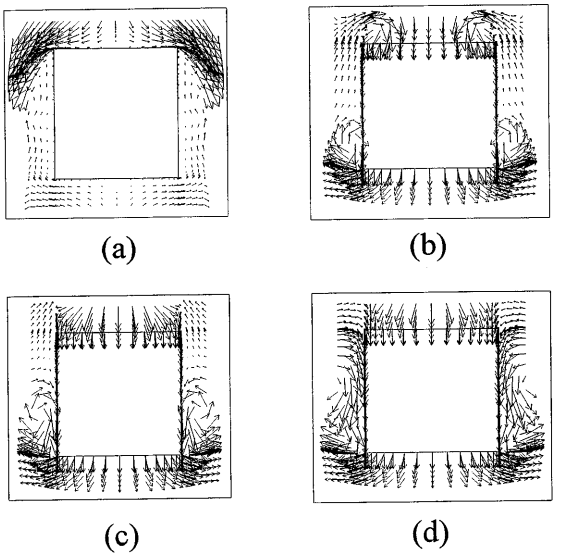

Fig. 8a–d. The transient developments of the velocity vectors around the body for Re = 500 and $V_b = -2.0$ case **a** $\tau = 0.0$, **b** $\tau = 0.25$, **c** $\tau = 0.5$, **d** $\tau = 1.0$

for the fluids near the top surface of the body, since the moving velocity of the body is greater than the approaching velocity of the fluids, the fluids complement the vacant space induced by the movement of the body not only from the approaching fluids but also from the fluids near the lateral surface of the body in the early stages of the transient developments. The fluids can not catch up with the top surface of the body and new recirculation zones are formed around the corners of the top surface, which is disadvantageous to heat transfer. After that, most of the fluids that complement the vacant space induced by the movement are provided from the approaching fluids, which is like the situation of the fluids impinging on the top surface of the body. As a result, the recirculation zones are vanished, and the phenomena are different from those of the above case as shown in Fig. 3 and enhance the heat transfer rate.

The transient developments of the average local Nusselt numbers $\overline{Nu_X}$ and $\overline{Nu_Y}$ for $V_b = -2.0$ case are shown in Fig. 9. Based upon the reasons mentioned above, the variations of the average local Nusselt numbers on the bottom surface of the body are similar to those of

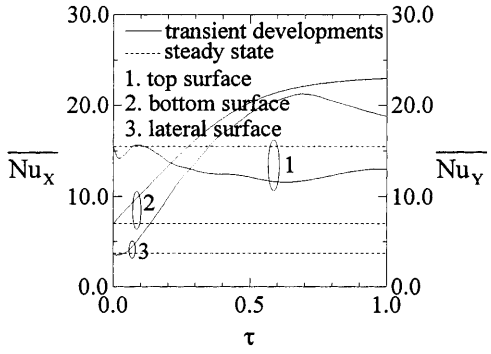

Fig. 9. The transient developments of the average local Nusselt numbers on the surfaces of the body for Re = 500 and $V_b = -2.0$ case

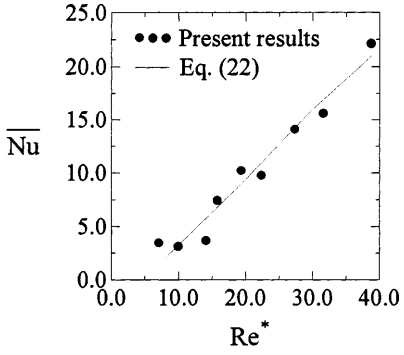

Fig. 10. The relationships of the mean global Nusselt numbers $\overline{Nu}$ and the special Reynolds number Re^*

the case of $V_b = -0.5$. As for the top surface of the body, because the fluids hardly impinge on the top surface and the recirculation zones are formed around the corner of the top surface at first, the average local Nusselt numbers distributed on the top surface are decreased. As the time increases, the recirculation zones around the corner of the top surface are vanished, and the average local Nusselt numbers distributed on the top surface then increase a little. As for the lateral surface, the average local Nusselt numbers are increased at the beginning. As the time τ is about larger than 0.7, the fluids near the lateral surface flow with the lateral surface and the reattachment region is destroyed, which causes the heat transfer rates reduced. From the variations of heat transfer mentioned above, the mean increment of the average global Nusselt numbers Nu in the computing range is about 105%, which is larger than that of $V_b = -0.5$ case.

Furthermore, three different Reynolds numbers of Re = 100, 500 and 750 with three different body moving velocities of $V_b = -0.5$, -1.0 and -2.0 are taken into consideration to determine the relationships among the three variables of the mean global Nusselt number $\overline{Nu}$, Reynolds number Re and the moving velocity of the body V_b in the computing range. For convenience of expression, the results shown in Fig. 10 are presented in terms of a special Reynolds number Re^*,

$$Re^* = \frac{\nu_0 l}{\nu} \cdot \left| \frac{\nu_b}{\nu_0} \right| = Re|V_b| \qquad (21)$$

The relationships can be approximately correlated by Eq. (22).

$$\overline{Nu} = 0.62\, Re^{*1/2} - 2.95 \qquad (22)$$

5 Conclusions

Flow fields and heat transfer of a body moving in the same direction as the flowing fluids are investigated numerically. The results can be summarized as follows:

1. The fluids near the top and lateral surfaces of the body simultaneously complement the vacant space induced by the movement of the body, and new recirculation zones are formed near the corners of the top and lateral surfaces of the body. These phenomena are apparently different from those of the body fixed in the flowing fluids.
2. The heat transfer rates of the body moving in the same direction with the flowing fluids are enhanced significantly as the body moving faster, but almost without enhancement as the moving velocity of the body is slower.
3. The relationships between the mean global Nusselt number $\overline{Nu}$ of the body and the special Reynolds number Re^* is a positive correlation.

References

1. **Hirt CW; Amsden AA; Cooks HK** (1974) An arbitrary Lagrangian–Eulerian computing method for all flow speeds. J Comput Phys 14: 227–253
2. **Hughes TJR; Liu WK; Zimmermann TK** (1981) Lagrangian–Eulerian finite element formulation for incompressible viscous flows. Comput Meth Appl Mech Eng 29: 329–349
3. **Ramaswamy B** (1990) Numerical simulation of unsteady viscous free surface flow. J Comput Phys 90: 396–430
4. **Soulaimani A; Saad Y** (1998) An arbitrary Lagrangian-Eulerian finite element method for solving three-dimensional free surface flows. Comput Meth Appl Mech Eng 162: 79–106
5. **Donea J; Giuliani S; Halleux JP** (1982) An arbitrary Lagrangian–Eulerian finite element method for transient dynamic fluid structure interactions. Comput Meth Appl Mech Eng 33: 689–723
6. **Huerta A; Liu WK** (1989) Viscous flow structure interaction. J Pressure Vessel Technol 110: 15–21
7. **Nomura T** (1993) Finite element analysis of vortex-induced vibrations of bluff cylinders. J Wind Eng Ind Aerodynamics 46: 587–594
8. **Masud A; Hughes TJR** (1997) A space-time Galerkin/least-squares finite element formulation of the Navier–Stokes equation for moving domain problems. Comput Meth Appl Mech Eng 146: 91–126
9. **Liu WK; Chang H; Chen JS; Belytschko T** (1988) Arbitrary Lagrangian-Eulerian Petrov–Galerkin finite elements for nonlinear continua. Comput Meth Appl Mech Eng 68: 259–310
10. **Chippada S; Jue TC; Ramaswamy B** (1995) Finite element simulation of combined buoyancy and thermocapillary driven convection in open cavities. Int J Numer Meth Eng 38: 335–351
11. **Harber RB** (1984) A mixed Eulerian–Lagrangian displacement model for large-deformation analysis in solid mechanics. Comput Meth Appl Mech Eng 43: 277–292
12. **Wang J; Gadala MS** (1997) Formulation and survey of ALE method in nonlinear solid mechanics. Finite Ele Anal Design 24: 253–269

13. **Reddy JN; Gartling DK** (1994) The Finite Element Method in Heat Transfer and Fluid Dynamics. Ann Arbor: CRC Press Inc
14. **Fu WS; Shieh WJ** (1992) A numerical study of transient natural convection under time-dependent gravitational acceleration field. Wärme-Stoffübertrag 27: 109–117
15. **Schlichting H** (1979) Boundary Layer Theory. 7th ed., New York: McGraw-Hill